Applied Catalysis B: Environmental 200 (2017) 543–551

Contents lists available at ScienceDirect

Applied Catalysis B: Environmental

journal homepage: www.elsevier.com/locate/apcatb

Efficient formaldehyde oxidation over nickel hydroxide promoted Pt/γ-Al_2O_3 with a low Pt content

Tengfei Yang[a,b,c], Ying Huo[a,b,c], Yang Liu[b,c], Zebao Rui[a,c,*], Hongbing Ji[b,c,*]

[a] School of Chemical Engineering and Technology, Sun Yat-sen University, Guangzhou 510275, PR China
[b] School of Chemistry and Chemical Engineering, Sun Yat-sen University, Guangzhou 510275, PR China
[c] R&D Center of Waste-gas Cleaning & Control, Huizhou Research Institute of Sun Yat-Sen University, Huizhou 516081, PR China

ARTICLE INFO

Article history:
Received 19 April 2016
Received in revised form 24 June 2016
Accepted 22 July 2016
Available online 22 July 2016

Keywords:
Catalytic oxidation
Platinum
Formaldehyde
Alumina
Nickel hydroxide interface

ABSTRACT

Rational design of efficient noble metal catalysts and its application process by the interface promoted strategy is an emerging research field. Herein, highly efficient nickel hydroxide promoted PtNi(OH)x/γ-Al_2O_3 catalysts for room temperature HCHO oxidation was developed. PtNi(OH)x/γ-Al_2O_3 demonstrates remarkably better performance than the state of the art non-reductive oxide supported Pt catalysts, and ranges among the best performance of the reductive metal oxide supported Pt catalysts. A (>)99% HCHO conversion and a (>)100 h stable performance at 30 °C were obtained over PtNi(OH)x/γ-Al_2O_3 with a 0.3 wt% Pt loading amount. Various characterizations, including in situ DRIFTS study, were performed to understand the reason for the enhanced performance of PtNi(OH)x/γ-Al_2O_3. The superior performance is attributed to the formation of enormous Pt/Ni(OH)x interface, and the preferred hydroxyl facilitated HCHO oxidation pathway through formate oxidation by the abundant associated hydroxyl groups nearby the Pt active sites. Such hydroxyl groups confined interface promotion strategy may bring new insight into the designing of highly efficient bimetallic catalysts and its potential technological applications for HCHO removal.

1. Introduction

Formaldehyde (HCHO) is a dominant indoor air pollutant which is harmful to human health even at a very low concentration. Various methods have been studied to reduce indoor HCHO pollution, such as adsorption, photocatalysis and thermal catalysis, among which catalytic oxidative decomposition of HCHO to CO_2 and H_2O at room temperature is considered to be the most promising strategy because this process is environmentally friendly and energy saving [1,2]. It is generally agreed that supported noble metal catalysts exhibit high HCHO oxidation activity, and reducible oxides, such as TiO_2 [3–10], CeO_2 [12–14], MnO_2 [15,16] and Co_3O_4 [17], are used as the support of preferable choice. This is because a reducible oxide has strong surface interactions with the supported metal which help to stabilize high dispersions of noble metal particles. Such interaction might cause the charge transfer between the supported metal and the support, which provides active oxygen species for the reaction [4–7,12]. It is believed that the surface oxygen species have key roles in low temperature HCHO oxidation [3–7,12–14]. As a result, the complete HCHO conversion into CO_2 and H_2O at room temperature was frequently reported over the reducible oxide supported catalysts, such as Pt/TiO_2 [3–10], Pt/MnOx-CeO_2 [11], and Au/CeO_2 [12].

Aside from HCHO oxidation, alumina is usually adopted as a support material of preferable choice due to its great advantages, such as high surface area, thermal and chemical stability and low cost. However, alumina was considered as a poor support for low temperature HCHO oxidation catalysts due to its irreducibility [15,18–20]. For instance, early reports showed that the catalytic activities of the Al_2O_3 supported Pt catalysts were unsatisfied for low-temperature oxidation of HCHO, requiring either heating or high Pt loading amount (>or = 1 wt%) for a complete HCHO conversion [18–20]. Benefit from the understanding of the alternative HCHO oxidation pathway by the promotion of surface hydroxyls [8], some groups attempted to improve the performance of the supported metal catalysts by enriching the surface hydroxyls groups of the catalysts [8–10], including the alumina supported catalysts [21,22]. Chen et al. [21] found that the surface hydroxyls of γ-Al_2O_3 played an important role in the HCHO oxidation, thus, the presence of water enhanced the HCHO conversion over Au/γ-Al_2O_3. Xu

* Corresponding authors at: School of Chemical Engineering and Technology, Sun Yat-sen University, Guangzhou 510275, PR China.
E-mail addresses: ruizebao@mail.sysu.edu.cn (Z. Rui), jihb@mail.sysu.edu.cn (H. Ji).

http://dx.doi.org/10.1016/j.apcatb.2016.07.041
0926-3373/

et al. [22] reported nanostructured AlOOH supported Pt catalysts were more active for the oxidative decomposition of HCHO than the conventional commercial γ-Al_2O_3 supported Pt catalyst due to the function of hydroxyls.

It is widely agreed that the existence of surface hydroxyls near to noble metal particles is beneficial for the oxidation of HCHO [8–10,21,22]. However, the conventional tailoring of the surface hydroxyls, such as depositing of metal nanoparticles over hydroxyls enriched support [22,23], the addition of alkalis [8,9] or the introduction of water to the reaction system [10,21,24] introduced rather limited metal-metal hydroxide interfaces and performance promotion. In recent years, rational design of metal-metal oxide [25–27] or metal-metal hydroxide interfaces [28–30] has been demonstrated as an effective method to improve the performance of the heterogeneous catalysts in many reaction systems. For instance, Subbaraman et al. [28] reported an enhancing hydrogen evolution activity in water splitting by tailoring Li^+-$Ni(OH)_2$-Pt interfaces. Chen et al. [30] developed an alloy-assisted strategy to produce a practical Pt nanocatalyst with catalytic M-OH-Pt (M = Ni and Fe) sites, which were highly efficient for carbon monoxide (CO) oxidation at room temperature. By rational tailoring the Pt/Ni(OH)x interface, we show here that low loading of Pt over commercial γ-Al_2O_3 can be as effective as (or more efficient than most of) the well-developed reducible oxide supported Pt catalysts for HCHO oxidation. A highly efficient nickel hydroxide promoted PtNi(OH)x/γ-Al_2O_3 catalysts for trace HCHO oxidation was developed by a two-step wet-chemical method, namely fabricating PtNi(OH)x nanoparticles followed by the dispersion over the γ-Al_2O_3 support. PtNi(OH)x/γ-Al_2O_3 with a 0.3 wt% Pt loading amount demonstrated a HCHO conversion of (>)99% with a (>)100 h stable performance at 30 °C. The mechanism leading to its high catalytic activity and stability were studied by various characterizations, including in situ DRIFTS study. The superior performance is related to the formation of enormous Pt/Ni(OH)x interface. Such hydroxyl groups confined interface promotion strategy represents a powerful approach towards designing high-performance heterogeneous catalysts for HCHO removal.

2. Experimental

2.1. Preparation of Pt-based nanoparticles

The procedure for the Pt-based nanoparticles (NPs) preparation by a wet-chemical method follows the established procedures in the literature with some modification [30]. Platinum acetylacetonate [$Pt(acac)_2$, 97%], Nickel acetylacetonate [$Ni(acac)_2$, 95%], Oleylamine (OAm, 80–90%) and *n*-butylamine (98%) were purchased from Aladdin and used as received without further purification. In a typical synthesis of cuboctahedral Pt NPs, 10 mg $Pt(acac)_2$ (0.02425 mmoL) and 5 mL oleylamine were mixed together in a three round-bottomed flask with a capacity of 50 mL, and then heated at 343 K for 10 min to form a homogeneous yellow solution. Then the sealed flask was charged with CO to 1 bar and then heated at 453 K for 40 min before it was cooled to room temperature. The products were precipitated using ethanol, separated via centrifugation and further purified using a cyclohexane-ethanol solution. PtNi NPs were synthesized with a similar process by dissolving the precursors $Pt(acac)_2$ (10 mg, 0.02425 mmoL) and $Ni(acac)_2$ (5 mg, 0.0185 mmol) in 5 mL oleylamine solution and then heated at 343 K until a transparent solution was obtained. Then the sealed flask was charged with CO to 1 bar and heated from 343 K to 513 K in about 50 min and kept at 513 K for 60 min. The products were precipitated using ethanol, separated via centrifugation and further purified using a cyclohexane-ethanol solution after it was cooled to room temperature. The Pt/Ni molar ratio of the as- prepared PtNi NPs with a value of 1.3 was confirmed by flame atomic absorption spectrometry (Z-2000, Hitachi).

2.2. Preparation of catalysts

Pt/γ-Al_2O_3 and PtNi/γ-Al_2O_3 catalysts were prepared by a two-step wet chemical method, namely fabricating Pt or PtNi NPs with the aforementioned procedure followed by the dispersion over the γ-Al_2O_3 support. In order to avoid the possible effect of the surface containment (mainly organic species) and microstructural change during the catalyst preparation process of the as-received γ-Al_2O_3 powders, the support γ-Al_2O_3 (Sinopharm Chemical Reagent Co., China) was calcined in air at 900 °C for 6 h prior to the use. In a typical catalyst preparation process, the Pt-based NPs were first dissolved in *n*-butylamine to form a homogeneous suspension with a concentration of ~10 mg Pt per 25 mL solvent. The γ-Al_2O_3 support was then added to the aforementioned *n*-butylamine solution and stirred in air at room temperature for three days. The amount of support added was calculated from the desired loading of Pt. The solids were then precipitated using ethanol, separated via centrifugation and then washed with ethanol for several times to remove the excess *n*-butylamine. The catalysts were then dried in a vacuum drying box at 70 °C. Finally, the catalyst was heated from room temperature to 200 °C in 6 h and kept at 200 °C for 1 h in air. The as prepared catalysts were denoted as Pt/γ-Al_2O_3 and PtNi/γ-Al_2O_3 with a Pt weight loading amount number in front for simplicity. As references, 0.2% Pt/γ-Al_2O_3(IM) and 0.2% PtNi/γ-Al_2O_3(IM) with a molar ratio of Pt/Ni = 1.3 were prepared by the conventional impregnation method. γ-Al_2O_3 support was impregnated in an aqueous solution containing the requisite amount of $Ni(NO_3)_2{\cdot}6H_2O$ (98.0%, Tianjin Damao Chemical Reagent Factory, China) for 1 h under ultrasonication. The as-impregnated sample was dried at 100 °C overnight and then calcined at 500 °C for 6 h in air with a heating rate of 10 °C/min. Then γ-Al_2O_3 and NiO/γ-Al_2O_3 support were impregnated in an aqueous solution containing the requisite amount of $H_2PtCl_6{\cdot}6H_2O$ (Alfa Aesar), respectively. The impregnated samples were dried at 200 °C for 1 h in air with a heating rate of 0.5 °C/min. Before reaction and characterization, all the catalysts were reduced by formaldehyde solution [31]. In this process, about 0.5 g of the as-calcined catalyst was added into 20 mL deionized water and 5 mL HCHO solution (~35 wt.% HCHO) and stirred for about 3 h under reflux conditions at 70 °C. The sample was then separated, washed with distilled water to remove any impurities on the surface of the catalyst and dried in air at 120 °C for 6 h for use. Final concentration of Pt and Ni in the samples was confirmed by flame atomic absorption spectrometry (Z-2000, Hitachi).

2.3. Catalysts characterization

Transmission electron microscopy (TEM, FEI Tecnai G2 Spirit) was used for the observation of NPs and their size distribution. High-angle annular dark-field (HAADF) imaging in the scanning transmission electron microscopy (STEM) mode was performed on the same electron microscope tilting the sample about a single axis using a Fischione ultra-narrow gap tomography holder. The phase purity and crystal structure of the catalysts were examined by X-ray diffraction (XRD, D-MAX 2200 VPC) using monochromatic CuKa radiation. BET surface area, pore size and pore volume of the sample were determined by N_2 adsorption isotherms at −196 °C over ASAP 2020 adsorption equipment. Before N_2 adsorption experiment, the sample was degassed at 200 °C for 3 h under vacuum. CO chemisorption analysis was performed at 35 °C using a Micromeritics ASAP 2020C automated system. Before CO chemisorption, the sample was first evacuated at 10^{-6} mm Hg and 110 °C for 30 min followed by the reduction under flowing H_2 at 200 °C for 30 min.

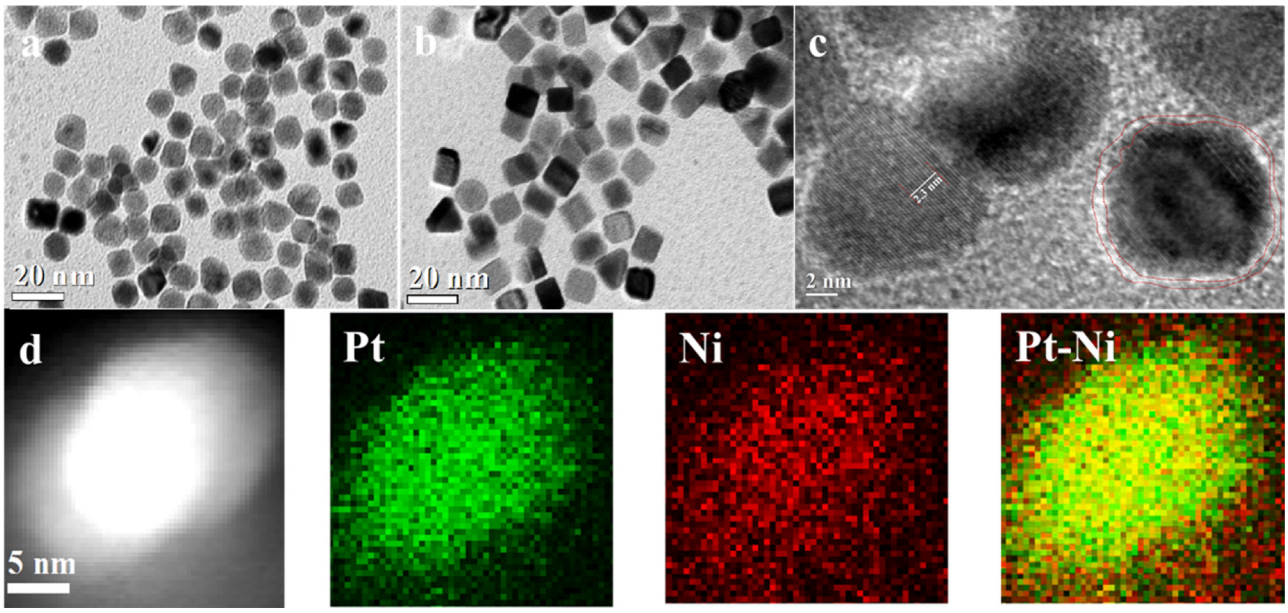

Fig. 1. STEM images of (a) Pt and (b&c) PtNi nanoparticles (NPs), and (d) EDS elemental mapping of PtNi nanoparticle.

A CO/Pt average stoichiometry of 1 was assumed for the calculation of dispersion. X-ray photoelectron spectroscopy (XPS) analysis was conducted on a ESCALAB 250 spectrometer (Thermo Fisher Scientific, Al Kα monochromate, $h\nu$ = 1486.6 eV) under a vacuum of $\sim 2 \times 10^{-7}$ Pa. Charging effects were corrected by adjusting the main C 1s peak to a position of 284.8 eV. CO-TPR was performed in a tubular (i.d.=7 mm) fixed-bed reactor, and about 50 mg sample was used in each test. The sample was first preheated under an air flow of 30 mL/min at 200 °C for 1 h, followed by purging with He at 200 °C for 1 h and cooling down to room temperature. The flow of 5% CO in He (50 mL/min) was then switched into the system, and the sample was heated up to 200 °C from room temperature at a rate of 5 °C/min. The amount of CO in the stream during the reduction was measured with a mass spectrometry (MS; Hidden HPR 20) at m/e = 28. Fourier transform infrared spectra (FTIR) were collected using a Bruker Tensor 37 FTIR Spectrometer in the frequency range of 4000–400 cm^{-1}. About 1 mg of sample was mixed in an agate mortar with ~300 mg of Perkin Elmer's potassium bromide followed by a thorough drying under a heat lamp. The mixture was then pressed into a pellet die for 5 min using a force of 5 tons, and transparent pellets were obtained for FTIR tests. In situ Diffuse Reflectance Infrared Fourier Transformed Spectroscopy (DRIFTS) analysis used in this study was performed on EQVINOX-55 FFT spectroscope apparatus (Bruker), equipped with a diffuse reflectance accessory and a Mercury Cadmium Telluride (MCT) detector. About 10 mg finely ground sample was packed in the ceramic crucible of the in situ chamber. 100 mL/min He or reactant stream (He/O_2 = 4) containing HCHO and water vapor (~35% relative humidity) was introduced. The spectra under reaction conditions were recorded after 64 scans with a resolution of 4 cm^{-1}. The in situ DRIFT spectrum in He flow at room temperature was measured and taken as a background for each sample. The effluent species were monitored with a mass spectrometry (MS; Hidden HPR 20) to monitor CO_2 at m/e = 44.

2.4. HCHO catalytic oxidation

A quartz tubular (i.d.=7 mm) fixed-bed reactor was used for the catalytic oxidation of HCHO under atmospheric pressure. Approximately 0.2 g of the catalyst with particle size of 177–250 μm was packed. The reactant is composed of a simulated air stream (N_2/O_2 = 4, 80 mL/min), ~30 ppm HCHO and water vapor (~35% relative humidity). Gaseous HCHO was generated by passing a stream of simulated air through a bubbler containing a HCHO solution (35 wt.% HCHO). Experiments were performed at GHSV (gas hourly space velocity) of 24000 (or 48000 and 72000 for the effect of GHSV study) ml h^{-1} g^{-1}. HCHO concentration in the reactant or product gas stream was analyzed by phenol spectrophotometric method [5–7]. The conversion of HCHO was calculated based on the concentration change.

3. Results and discussion

3.1. Structural properties

Fig. 1a–b shows the STEM images of the as-synthesized Pt and PtNi NPs with a mean diameter around 11 nm. The high resolution image of the PtNi NPs in Fig. 1c. presents both Pt core with interplanar lattice fringes distance of 0.23 nm, corresponding to Pt (111) planes, and the obvious boundary around the Pt core. The EDS elemental mapping of the PtNi NP in Fig. 1d shows that this layer contains nickel. The XPS spectra of Pt and PtNi NPs are presented in Fig. 2. The core level of Pt $4f_{7/2}$ (ca. 70. 8 eV) demonstrates the metallic state of Pt in Pt and PtNi NPs [5,30]. The O1s spectrum of PtNi NPs displays two peaks at 532.8 and 530.7 eV, which are ascribed to oxygen of OH (Ni—OH) and bridging oxo-groups (Ni—O—Ni) with an A_{OH}/A_O ratio of 4.8. The $Ni2p_{3/2}$ peak can be deconvoluted into two peaks at 852.2 and 855.4 eV associated well with the Ni^0 and $Ni(OH)_2$ species [32,33], with an $A_{Ni(OH)2}/A_{Ni}$ ratio of 2.3. These results confirm the formation of nickel hydroxide promoted $PtNi(OH)_x$ nanoparticles.

The representative TEM images and EDS mapping of Pt and PtNi NPs loaded on γ-Al_2O_3 are presented in Fig. 3. As presented in Fig. 3a & c, homogeneous metal particle distribution can be clearly observed over the Pt/γ-Al_2O_3 and PtNi/γ-Al_2O_3, with the average metal particle size ~6.4 nm over Pt/γ-Al_2O_3 and ~5.7 nm over PtNi/γ-Al_2O_3, respectively. The EDS mappings (Fig. 3b & d) further confirms the homogeneous Pt and Ni distribution, and the well PtNi combination over the Pt/γ-Al_2O_3 and PtNi/γ-Al_2O_3. In contrast, the Pt particles over Pt/γ-Al_2O_3(IM) and PtNi/γ-Al_2O_3(IM) prepared by the conventional impregnation method are difficult to be calculated due to the low Pt loading amount and good Pt

Table 1
Specific surface area, average pore size, pore volume, Pt apparent dispersion and particle size of 0.2 wt% Pt-based catalysts.

Sample	BET surface area (m^2/g)	average pore width (nm)[a]	Pore volume (cm^3/g)[b]	d_{CO} (nm)[c]	Pt apparent dispersion (%)[c]
γ-Al_2O_3	94	15.5	0.46	–	–
Pt/γ-Al_2O_3(IM)	97	15.8	0.46	2.27	49.8
PtNi/γ-Al_2O_3(IM)	81	14.2	0.42	1.94	58.3
Pt/γ-Al_2O_3	93	14.5	0.37	3.10	36.5
PtNi/γ-Al_2O_3	91	13.6	0.35	2.92	38.7

[a] BJH desorption average pore width.
[b] The desorption pore volume for the 1.7–300 nm range of pore diameters.
[c] Average Pt particle size and apparent dispersion calculated by CO chemisorption assuming that the metal particle to be hemisphere.

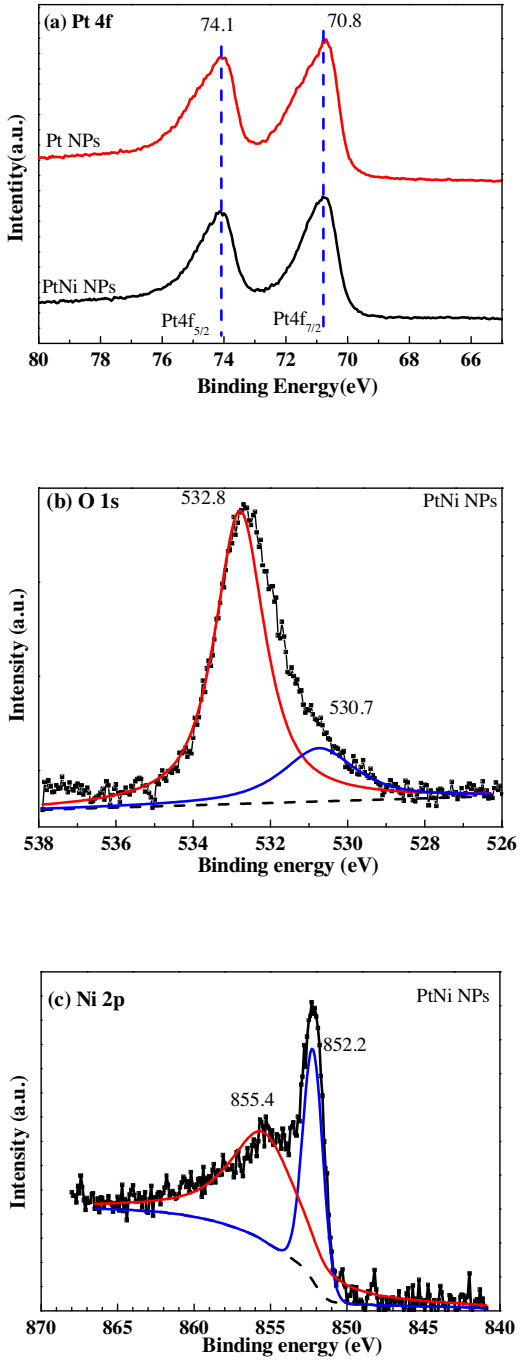

Fig. 2. XPS analysis of Pt and PtNi nanoparticles (NPs): Pt 4f, O 1s and Ni 2p.

Table 2
XPS data of 0.2 wt.% Pt-based catalysts.

Sample	BE/eV				Surface atom ratio[a]
	$Pt4d_{5/2}$	Al2p	$Ni2p_{3/2}$	O_{OH} (O_O)	O_{OH}/O_O
Pt/γ-Al_2O_3(IM)	311.7	74.0	–	532.2(530.7)	0.64
PtNi/γ-Al_2O_3(IM)	311.3	74.0	854.7	532.1(530.7)	0.62
Pt/γ-Al_2O_3	314.1	73.9	–	532.5(530.7)	1.05
PtNi/γ-Al_2O_3	313.1	74.0	855.3	532.7(530.7)	1.01

[a] Calculated from the corresponding areas of fitted peaks done by XPSPEAK 4.1 with Shirley background.

dispersion over the samples, as shown in Fig. S1 (supporting information). Table 1 lists the specific surface area, average pore size, pore volume and platinum dispersion of the samples. As listed, there is no obvious difference in the BET area among these samples. The Pt dispersion of Pt/γ-Al_2O_3 and PtNi/γ-Al_2O_3 prepared by the two-step wet-chemical method is generally lower than the corresponding Pt/γ-Al_2O_3(IM) and PtNi/γ-Al_2O_3(IM) samples, which is consistent with the TEM observation. The introduction of nickel can improve the Pt dispersion over γ-Al_2O_3 to some extent. The Pt dispersions measured by CO chemisorption for Pt/γ-Al_2O_3 and Pt/γ-Al_2O_3(IM) are 36.5% and 49.8%, which increase to 38.7% and 58.3% for PtNi/γ-Al_2O_3 and PtNi/γ-Al_2O_3(IM), respectively. The XRD patterns of these Pt-based catalysts are displayed in Fig. 4a shows the FTIR spectra of Pt/γ-Al_2O_3, PtNi/γ-Al_2O_3, Pt/γ-Al_2O_3(IM), PtNi/γ-Al_2O_3(IM) and γ-Al_2O_3 support. A strong and broad band at ca. 3450 cm^{-1} and a sharp peak at ca. 1640 cm^{-1} in the spectra of all the Pt based catalysts can be assigned to the stretching and bending vibrations of OH, respectively. Since the samples were fully dried prior to the FTIR tests, the characteristic bands of OH indicate the presence of a large amount of hydroxyl groups on the surfaces of these samples [22]. Generally, the catalysts prepared by the two-step wet-chemical method show more intense OH vibration bands or higher surface OH amount than the corresponding Pt/γ-Al_2O_3(IM) and PtNi/γ-Al_2O_3(IM) samples. The chemical states of the surface elements were identified by XPS analysis, as shown in Fig. 5b, Figs. S2–4 (supporting information) and listed in Table 2. The O 1 s spectra of theses catalysts in Fig. 5b show two peaks located at 530.7 and 532.1–532.7 eV assigned to the lattice oxygen (O_O) of γ-Al_2O_3 or bridging oxo-groups (Ni—O—Ni) and the oxygen of the surface hydroxyl (O_{OH}) groups, respectively [22,34]. The quantitative analysis shows that the surface O_{OH} concentration over Pt/γ-Al_2O_3 and PtNi/γ-Al_2O_3 prepared by the two-step wet-chemical method are generally higher than the corresponding Pt/γ-Al_2O_3(IM) and PtNi/γ-Al_2O_3(IM) prepared by the conventional impregnation method, which are consistent with the above FTIR results. For instance, the O_{OH}/O_O peak area ratios are 0.62 and 1.01 over PtNi/γ-Al_2O_3(IM) and PtNi/γ-Al_2O_3, respectively. The Pt4f peaks of these γ-Al_2O_3 supported catalysts are not observed due to the weak peak of $Pt4f_{5/2}$ (at ca.71–74.3 eV) overlapped by the strong peak of Al_{2p} (Fig. S2, supporting information) of γ-Al_2O_3 [34]. Alternatively, Pt $4d_{5/2}$ XPS spectra (Fig. S3, supporting information) show weak peaks at 311.3–314.1 eV, which are close to the

characteristic peak of Pt^0 (ca.314.7 eV) but not Pt^{2+} (ca. 317.3 eV) [19,35,36], indicating that the Pt species over these catalysts are mainly composed of Pt^0 species. The Ni XPS spectra (Fig. S4, supporting information) show weak $Ni2p_{3/2}$ peaks at ca. 855.3 eV for PtNi/γ-Al_2O_3, which is attributed to the Ni2p spectrum of $Ni(OH)_2$ [32,33], and ca. 854.7 eV for PtNi/γ-Al_2O_3 (IM), which is assigned to the NiO species [32]. Fig. 6 presents the CO-TPR profiles of Pt/γ-Al_2O_3, PtNi/γ-Al_2O_3, Pt/γ-Al_2O_3(IM) and PtNi/γ-Al_2O_3(IM), which shows a CO consumption peak at ca.54 °C over PtNi/γ-Al_2O_3, while no obvious CO consumption under the experimental conditions is observed over the other samples. As reported, the consumption of CO over PtNi/γ-Al_2O_3 was due to the couple of CO with —OH to produce CO_2 [30]. Thus, these results demonstrate the existence of enormous surface OH groups over PtNi/γ-Al_2O_3 and the oxidation ability of the interface OH groups.

3.2. Catalysts activity test

The catalytic activities of Pt/γ-Al_2O_3, PtNi/γ-Al_2O_3, Pt/γ-Al_2O_3(IM) and PtNi/γ-Al_2O_3(IM) are compared in Fig. 7. All samples are structured with γ-Al_2O_3 phase. No characteristic peaks of Pt or Ni based species were detected by the XRD due to the low and well-dispersed Pt or Ni in the catalysts.

Fig. 5a. As shown, the activities of Pt/γ-Al_2O_3 and PtNi/γ-Al_2O_3 prepared by the two-step wet-chemical method are remarkably higher than the corresponding Pt/γ-Al_2O_3(IM) and PtNi/γ-Al_2O_3(IM) catalysts prepared by the impregnation method. The introduction of Ni into the Pt catalyst can improve the performance of both Pt/γ-Al_2O_3 and Pt/γ-Al_2O_3(IM). When the Pt loading amount is 0.2 wt.%, the initial HCHO conversions at 30 °C are 8%, 38%, 50% and 93% over Pt/γ-Al_2O_3(IM), PtNi/γ-Al_2O_3(IM), Pt/γ-Al_2O_3, and PtNi/γ-Al_2O_3, respectively. Upon increasing the Pt loading amount up to 0.3 wt.%, a (>) 99% HCHO conversion is observed over PtNi/γ-Al_2O_3 during the temperature range of 30–80 °C. Further performance comparison of PtNi/γ-Al_2O_3 with PtNi/γ-Al_2O_3(IM, 200 °C), which used Ni/γ-Al_2O_3 prepared by the two-step wet-chemical method and calcined at 200 °C for the impregnation of Pt catalyst (See the supporting information for detail), was presented in Figs. S5 & 6 (supporting information). It is shown that both the surface OH concentration and initial activity over PtNi/Al_2O_3 (IM, 200 °C) are all significantly lower than those over PtNi/γ-Al_2O_3, confirming the importance of the formation of PtNi(OH)x interface for the oxidation of HCHO. Fig. 7b shows that 0.3% PtNi/γ-Al_2O_3 holds a good stability over the 100 h' test at 30 °C with a (>) 99% HCHO conversion. In order to further explore the applicability of the as-developed PtNi/γ-Al_2O_3 for low temperature HCHO oxidation, the performance of 0.2% PtNi/γ-Al_2O_3 at various space velocities were checked, as shown in Fig. 7c. Obviously, PtNi/γ-Al_2O_3 performs well even under a high gas hourly space velocity of 48,000 mL g^{-1} h^{-1}, with a HCHO conversion of 90% at room temperature. The effect of humidity on HCHO oxidation over PtNi/γ-Al_2O_3 at various temperatures of 30–80 °C was also studied and presented in Fig. S7(supporting information). It is found that 0.2% PtNi/γ-Al_2O_3 catalyst shows nearly 60% HCHO conversion in the dry feed gas (Relative humidity, RH% <5%) at 30 °C. Upon increasing the RH% to ~35%, the HCHO conversion increases up to 93% at 30 °C. The results indicate that the presence of water actually enhances the HCHO conversion through the function of surface or interface OH groups [10,23]. Finally, the performance of PtNi/γ-Al_2O_3 was compared with those typical Pt based catalysts listed in Table 3. As listed, the required Pt weight loading amounts for room temperature complete HCHO oxidation are ca.0.3% for PtNi/γ-Al_2O_3, 2% for Pt-FeO_x/γ-Al_2O_3 [19], 0.4% for Pt/ZSM-5 [23], 3% for Pt/MnO_x-CeO_2 [11] and 0.1%–1% for Pt/TiO_2 [3,5,6,8,10]. A general performance comparison with the reported data was presented in Table 3 by calculating Pt utilization efficiency (by normalizing the converted HCHO molecules to the packed Pt amount) at room temperature. As compared, even if the difference in experimental conditions is taken into consideration, the performance of the current PtNi/γ-Al_2O_3 is better than those reported Pt-FeO_x/γ-Al_2O_3 [19] and Pt/ZSM-5 [23] with irreducible support, and is among the best of those reducible support supported Pt catalysts [3,5,6,8,10,11,16]. These results convince the good performance and great application potential of PtNi/γ-Al_2O_3 catalyst for HCHO oxidation.

3.3. In-situ DRIFT test

In-situ DRIFTS test was performed to study the HCHO oxidation over Pt/γ-Al_2O_3(IM), PtNi/γ-Al_2O_3(IM), Pt/γ-Al_2O_3 and PtNi/γ-Al_2O_3. As shown in Fig.8a&b, after exposing the catalyst to O_2 + HCHO + He mixture gas at 30 °C and various adsorption time, the bands appear at 3265, 2991, 2941, 2895, 2820, 2780, 2510, 2340, 2042, 1715, 1570 and 1432 cm^{-1} over Pt/γ-Al_2O_3(IM) and PtNi/γ-Al_2O_3(IM). The bands at ca.2991 and 2780 cm^{-1} are assigned for δ_{CH} [37], and 2941, 2895 and 2820 cm^{-1} are attributed to ν_{CH} [8,37,38]. The bands at 1715 cm^{-1} and 1570 cm^{-1} are ascribed to ν_{CO} and $\nu_{(as)COO}$ of formate species, respectively [6–8,38]. The bands at ca. 3700–3000 cm^{-1} were attributed to OH group bonded to the catalyst surface or the adsorbed H_2O [8,22]. The formation of adsorbed CO_2 (band at 2340 cm^{-1}) [38] and CO (linearly adsorbed on Pt, Ca. 2042 cm^{-1}) were also observed [38]. Moreover, the small band at ca. 1432 cm^{-1} in the spectra is probably due to carbonate species, originating from the formate species oxidation over the catalyst [22]. The broad band at 2510 cm^{-1} corresponds to the head-to-head interaction of two COOH groups [39], indicating the accumulation of carboxyl groups over the catalysts surface. In comparison with the spectra for HCHO oxidation over Pt/γ-Al_2O_3(IM) and PtNi/γ-Al_2O_3(IM), the bands located at 3700–3000 cm^{-1} assigned to OH group are remarkably stronger over Pt/γ-Al_2O_3 and PtNi/γ-Al_2O_3 prepared by the two-step wet-chemical method, as shown in Fig. 8c & d. In addition, the bands at 2510 cm^{-1} belonging to the COOH groups and 2042 cm^{-1} corresponding to the adsorbed CO were not detected in Fig. 8c & d. Fig. 9shows in situ DRIFTS spectra of O_2 + HCHO + He gas mixture adsorption for 60 min at various temperatures over these samples. In general, the bands intensity of the intermediates, such as formate species, decrease with increasing adsorption temperature. In converse, the adsorbed CO_2 (2340 cm^{-1}) and surface carbonate species (1690 and 1320 cm^{-1}) [40] gradually increase with formate consumption. The corresponding effluent CO_2 flux during the in situ DRIFTS tests over PtNi/γ-Al_2O_3(IM) and PtNi/γ-Al_2O_3 at various temperatures were measured by online MS. As shown in Fig. S8 (supporting information), the CO_2 flux over both samples increases with increasing adsorption temperature. These results provide strong evidence for the deep oxidation of HCHO over these samples.

Fig. 10shows that the intensity of formate species band at 1570 cm^{-1} over the catalysts increases and gradually approaches to a steady level with increasing exposure time, while decreases with increasing adsorption temperature. The relative amount of accumulated formate species over these catalysts has a sequence of Pt/γ-Al_2O_3(IM) > (PtNi/γ-Al_2O_3(IM), Pt/γ-Al_2O_3) > PtNi/γ-Al_2O_3 under the same adsorption conditions, which is generally inverse to their activity sequence. Both the formate species formation rate from adsorbed HCHO and its decomposing or oxidation rate affect the surface formate species amount. In combination with the activity test results in Fig. 7, we can propose that the formate species decomposing/oxidation step is the controlling step, and both the fast formate species formation rate and decomposing/oxidation rate over PtNi/γ-Al_2O_3 result to its higher initial activity in

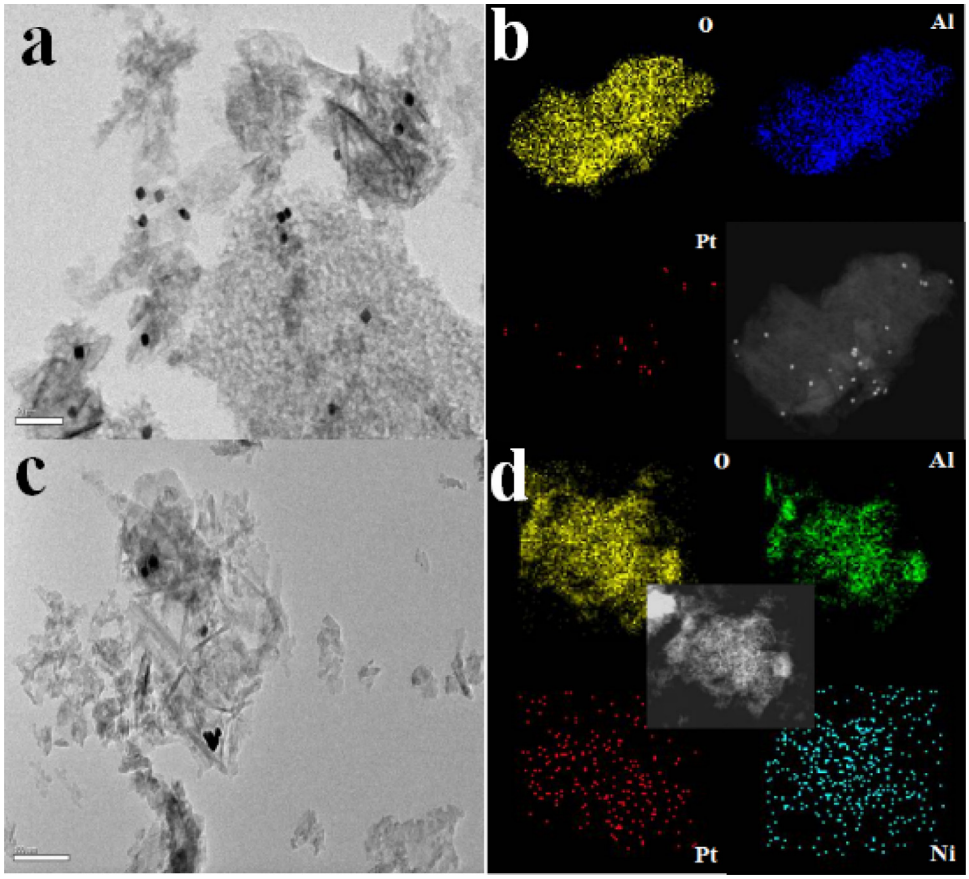

Fig. 3. STEM images and EDS elemental mappings of 0.2% Pt/γ-Al_2O_3 (a, b) and 0.2% PtNi/γ-Al_2O_3 (c, d).

comparison with those over Pt/γ-Al_2O_3, PtNi/γ-Al_2O_3(IM) and Pt/γ-Al_2O_3(IM). The viewpoint that formate species decomposing/oxidation step determines the HCHO oxidation rate over the noble metal catalysts also prevails in the literature [3–10,21].

4. Discussion

The direct adsorption and oxidation of HCHO over noble metal active sites or noble metal-metal oxide interface was proposed and demonstrated when a catalyst lacks OH groups [3–8]. In this route (HCHO → HCOO-M → CO-M + OH-M → $H_2O + CO_2$, M is noble metal), the decomposition of formate species to surface CO was regarded as the controlling step and the metal-support interaction played an important role [3–8]. Based on the characterization results obtained in this work, we can see that HCHO oxidation over PtNi/γ-Al_2O_3(IM) and Pt/γ-Al_2O_3(IM) generally follows this route due to the limited OH groups over the surface. Meanwhile, the poor Pt-support interaction due to the irreductive property of γ-Al_2O_3 leads to the poor performance of Pt/γ-Al_2O_3(IM) and PtNi/γ-Al_2O_3(IM) in comparison with the reductive TiO_2 supported Pt catalysts [4,7]. These observations are consistent with previous reports over the commercial γ-Al_2O_3 supported Pt catalysts [18–20].

However, when a large amount of nearby hydroxyls groups is present, an alternative hydroxyls facilitated HCHO oxidation route over the supported noble metal catalysts (HCHO → HCOO-M + OH-M → $H_2O + CO_2 + 2$ M, M is noble metal) was proposed and demonstrated [8–10,22]. In this route, the direct formate oxidation

Table 3
Performance comparison of the Pt-based catalysts for HCHO oxidation.

Catalyst	Noble metal Loading (wt%)	Space velocity ($mL\,h^{-1}g^{-1}$)	Inlet gas composition	R.T.[a]	HCHO conversion (%)	Pt utilization efficiency (s^{-1})	Ref.
$PtNi/Al_2O_3$	0.2	72000	~30 ppm HCHO, ~35%RH[a]	85	2.23×10^{-3}	This work	
$PtNi/Al_2O_3$	0.2	48000	~30 ppm HCHO, ~35%RH	90	1.57×10^{-3}	This work	
$PtNi/Al_2O_3$	0.3	24000	~30 ppm HCHO, ~35%RH	100	5.80×10^{-4}	This work	
Pt-0.3FeO_x/Al_2O_3	2	60000	~300 ppm HCHO, ~30%RH	63	1.37×10^{-3}	[19]	
Pt-1.0FeO_x/Al_2O_3	2	60000	~300 ppm HCHO, ~30%RH	100	2.18×10^{-3}	[19]	
Pt/TiO_2	0.4	30000	~50 ppm HCHO, ~35%RH	100	9.07×10^{-4}	[5]	
Pt/ZMS-5	0.4	30000	~50 ppm HCHO, ~35%RH	100	9.07×10^{-4}	[23]	
Pt/MnO_2/TiNT	0.2	30000	~50 ppm HCHO, ~35%RH	100	1.81×10^{-3}	[6]	
Pt/TiO_2	0.1	60000	~24 ppm HCHO, ~54%RH	100	3.48×10^{-3}	[10]	
Pt/TiO_2	1	60000	~24 ppm HCHO	100	3.48×10^{-4}	[10]	
Pt/MnO_x-CeO_2	3	30000	~30 ppm HCHO	100	7.25×10^{-5}	[11]	
Pt/MnO_2	2	20000	~ 460 ppm HCHO	30	3.34×10^{-4}	[16]	
Pt/TiO_2	1	50000	~100 ppm HCHO,	100	1.21×10^{-3}	[3]	
2%Na-Pt/TiO_2	1	120000	~600 ppm HCHO, ~50% RH	100	1.74×10^{-2}	[8]	

[a] RH: relative humidity, R.T.: room temperature.

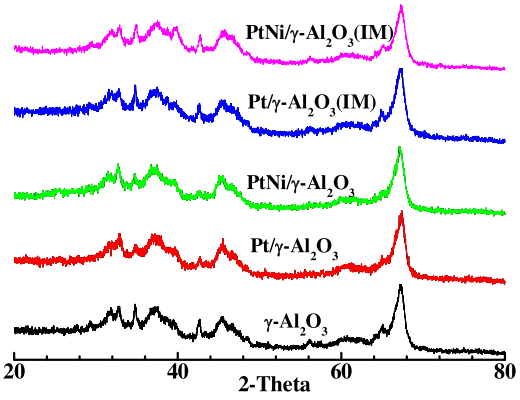

Fig. 4. XRD patterns of 0.2 wt.% Pt-based catalysts and γ-Al_2O_3.

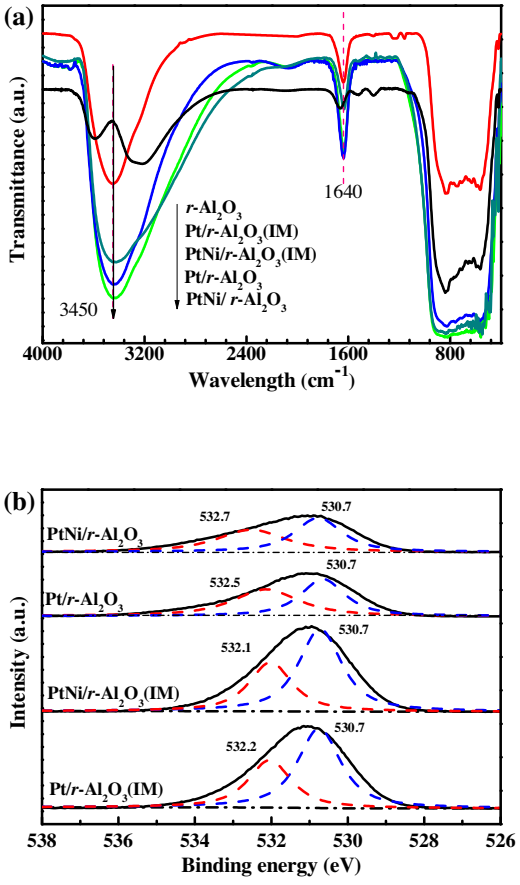

Fig. 5. FTIR spectra (a) and O1s XPS spectra (b) of 0.2 wt.% Pt-based catalysts.

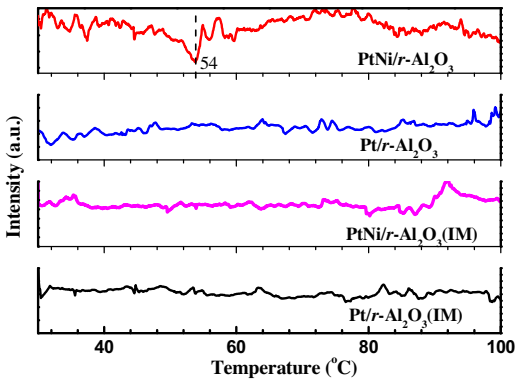

Fig. 6. CO-TPR profiles of 0.2 wt.% Pt-based catalysts.

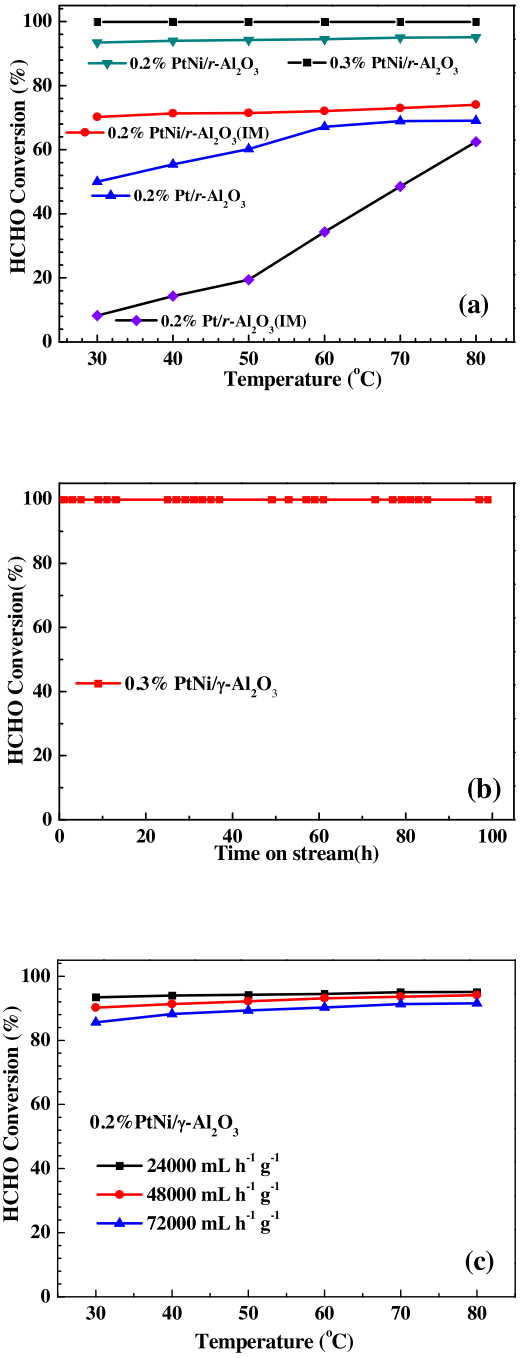

Fig. 7. (a) Dependence of HCHO conversion on reaction temperature for 0.2% Pt/γ-Al_2O_3(IM), 0.2% PtNi/γ-Al_2O_3(IM), 0.2% Pt/γ-Al_2O_3, 0.2% PtNi/γ-Al_2O_3, and 0.3% PtNi/γ-Al_2O_3, (b) Long term test over 0.3% PtNi/γ-Al_2O_3 at 30°, and (c) HCHO conversion over 0.2% PtNi/γ-Al_2O_3 at various GHSV and 30 °C.

with hydroxyls was regarded as the controlling step [8] and the existence of surface hydroxyls near to noble metal particles was beneficial for the oxidation of HCHO [8–10,21,22]. In addition, it was found that the reaction between surface hydroxyls and formate was preferred over the decomposition of formate to CO followed by CO oxidation route [8]. On the basis of the above results, we can find that the introduction of Ni^{2+} leads to the formation of PtNi(OH)x nanoparticles and enhances the nearby OH concentration over Pt particles surface, which agrees well with the stabilization role of Ni^{2+} in the Pt surface OH groups against dehydration reported previously [30]. It is found that HCHO oxidation over the hydroxyls or Ni(OH)x enriched PtNi/γ-Al_2O_3 generally follow the hydroxyls

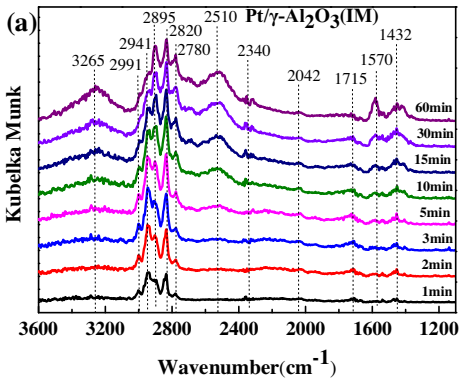

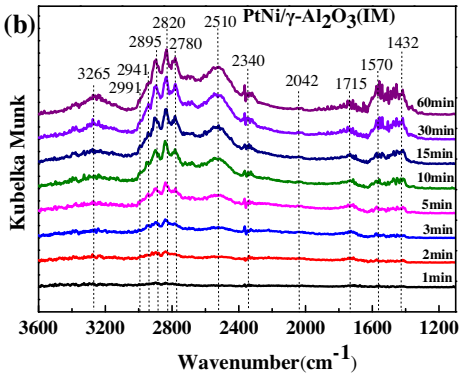

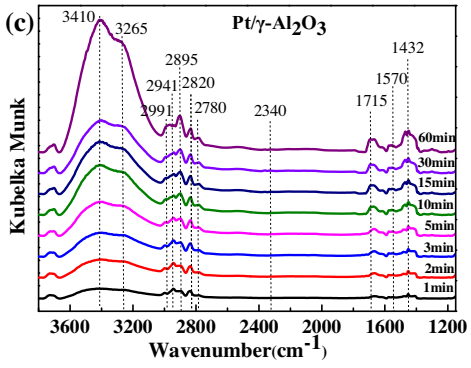

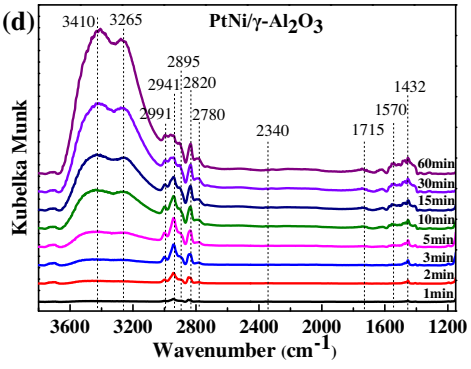

Fig. 8. In situ DRIFTS spectra of O_2 + HCHO + He gas mixture adsorption at 30 °C over (a) 0.2% Pt/γ-Al_2O_3(IM), (b) 0.2% PtNi/γ-Al_2O_3(IM), (c) 0.2% Pt/γ-Al_2O_3 and (d) 0.2% PtNi/γ-Al_2O_3.

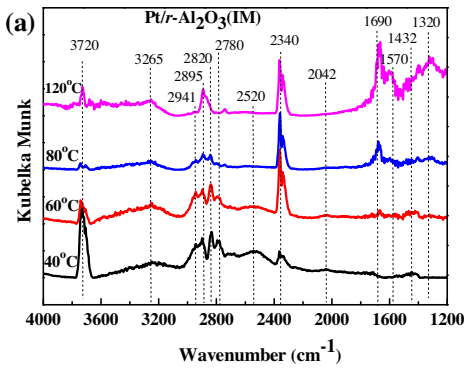

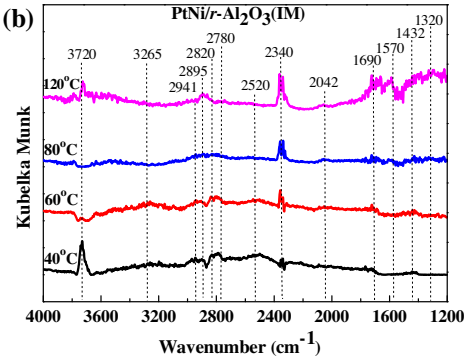

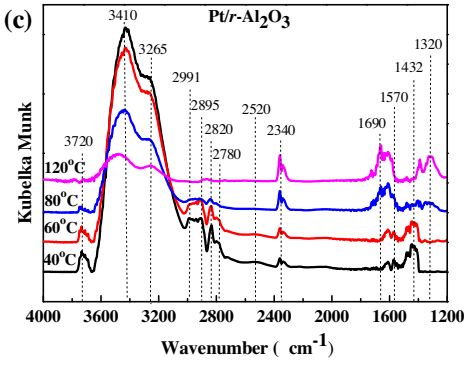

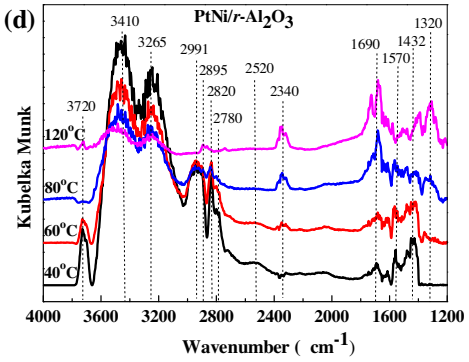

Fig. 9. In situ DRIFTS spectra of O_2 + HCHO + He gas mixture adsorption for 60 min at various temperatures over (a) 0.2% Pt/γ-Al_2O_3(IM), (b) 0.2% PtNi/γ-Al_2O_3(IM), (c) 0.2% Pt/γ-Al_2O_3 and (d) 0.2% PtNi/γ-Al_2O_3.

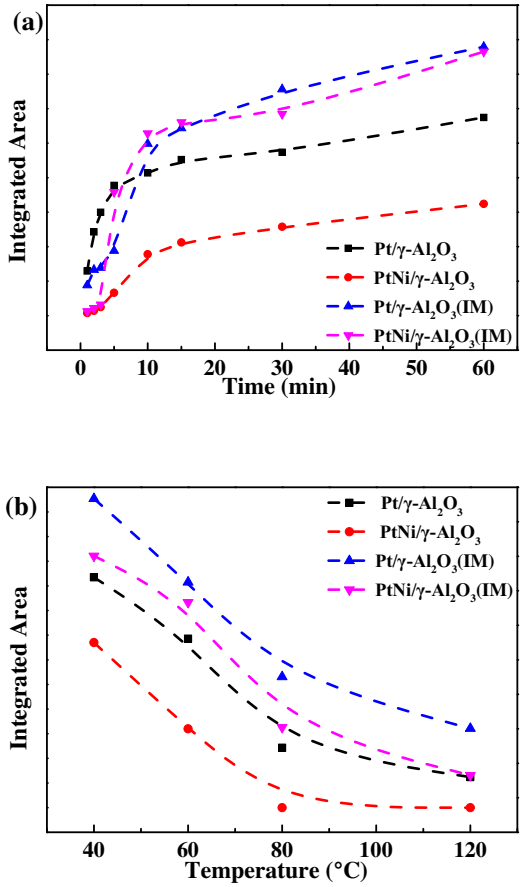

Fig. 10. (a) Intensity of 1570 cm^{-1} peak vs. time for different samples during O_2 + HCHO + He gas mixture adsorption at 30 °C, and (b) intensity of 1570 cm^{-1} peak vs. temperature for different samples during O_2 + HCHO + He gas mixture adsorption for 60 min.

facilitated route. The adsorbed formate is presumably oxidized into CO_2 by hydroxyls, mainly because no peak associated to molecularly adsorbed CO were observed in in situ DRIFTS spectra over PtNi/γ-Al_2O_3. As a result, the large amount of hydroxyls or Ni(OH)x connected to the Pt nanoparticles promotes the formate oxidation and finally greatly enhances the HCHO oxidation activity of PtNi/γ-Al_2O_3.

5. Conclusions

Highly efficient nickel hydroxide promoted PtNi(OH)x/γ-Al_2O_3 catalyst for trace HCHO oxidation was developed. PtNi(OH)x/γ-Al_2O_3 demonstrated better performance than the state of the art non-reductive oxide supported Pt catalysts, and ranged among the best performance of the reductive metal oxide supported Pt catalysts. A HCHO conversion of (>)99% with a (>)100 h stable performance was obtained at 30 °C over PtNi(OH)x/γ-Al_2O_3 with a 0.3 wt% Pt loading amount. The superior performance was related to the formation of enormous PtNi(OH)x interface, and the preferred hydroxyl facilitated HCHO oxidation pathway through formate oxidation by the abundant associated OH groups nearby the Pt sites. In short, the proposed hydroxyls (or hydroxide)-noble metal interface promoted strategy and developed PtNi(OH)x/γ-Al_2O_3 catalyst were demonstrated to be applicable for room temperature catalytic oxidation of HCHO.

Acknowledgements

The financial support by the Natural Science Foundation of China (21576298 and 21425627), Natural Science Foundation (2014A030313135 and 2014A030308012) and the Science and Technology Plan Project (2013B090500029 and 2014B090902006) of Guangdong Province and the State Key Laboratory of Chemical Resource Engineering (CRE-2015-C-301), China, is acknowledged.

Appendix A. Supplementary data

Supplementary data associated with this article can be found, in the online version, at http://dx.doi.org/10.1016/j.apcatb.2016.07.041.

References

[1] J. Pei, J.S. Zhang, Hvac&R Res. 17 (2011) 476–503.
[2] B. Bai, Q. Qiao, J. Li, J. Hao, Chin. J. Catal. 37 (2016) 102–122.
[3] C. Zhang, H. He, K.-i. Tanaka, Appl. Catal. B: Environ. 65 (2006) 37–43.
[4] H. Huang, D.Y.C. Leung, D. Ye, J. Mater. Chem. 21 (2011) 9647–9652.
[5] H. Chen, Z. Rui, H. Ji, Chin J. Catal. 36 (2015) 188–196.
[6] H. Chen, M. Tang, Z. Rui, H. Ji, Ind. Eng. Chem. Res. 54 (2015) 8900–8907.
[7] H. Chen, M. Tang, Z. Rui, X. Wang, H. Ji, Catal. Today 264 (2016) 23–30.
[8] C. Zhang, F. Liu, Y. Zhai, H. Ariga, N. Yi, Y. Liu, K. Asakura, M. Flytzani-Stephanopoulos, H. He, Angew. Chem. Int. Ed. 51 (2012) 9628–9632.
[9] L. Nie, J. Yu, X. Li, B. Cheng, G. Liu, M. Jaroniec, Environ. Sci. Technol. 47 (2013) 2777–2783.
[10] D.W. Kwon, P.W. Seo, G.J. Kim, S.C. Hong, Appl. Catal. B: Environ. 163 (2015) 436–443.
[11] X. Tang, J. Chen, X. Huang, Y. Xu, W. Shen, Appl. Catal. B: Environ. 81 (2008) 115–121.
[12] B. Chen, C. Shi, M. Crocker, Y. Wang, A. Zhu, Appl. Catal. B: Environ. 132 (2013) 245–255.
[13] H.-F. Li, N. Zhang, P. Chen, M.-F. Luo, J.-Q. Lu, Appl. Catal. B: Environ. 110 (2011) 279–285.
[14] B. Liu, C. Li, Y. Zhang, Y. Liu, W. Hu, Q. Wang, L. Han, J. Zhang, Appl. Catal. B: Environ. 111 (2012) 467–475.
[15] M. Álvarez-Galván, B. Pawelec, V. De la Peña O'shea, J. Fierro, P. Arias, Appl. Catal. B: Environ. 51 (2004) 83–91.
[16] X. Yu, J. He, D. Wang, Y. Hu, H. Tian, Z. He, J. Phys. Chem. C 116 (2011) 851–860.
[17] B. Bai, J. Li, ACS Catal. 4 (2014) 2753–2762.
[18] L. Wang, M. Sakurai, H. Kameyama, J. Hazard. Mater 167 (2009) 399–405.
[19] W. Cui, X. Yuan, P. Wu, B. Zheng, W. Zhang, M. Jia, RSC Adv. 5 (2015) 104330–104336.
[20] S. Colussi, M. Boaro, L. De Rogatis, A. Pappacena, C. de Leitenburg, J. Llorca, A. Trovarelli, Catal. Today 253 (2015) 163–171.
[21] B. Chen, X. Zhu, M. Crocker, Y. Wang, C. Shi, Catal.Commun. 42 (2013) 93–97.
[22] Z. Xu, J. Yu, M. Jaroniec, Appl. Catal. B: Environ. 163 (2015) 306–312.
[23] H. Chen, Z. Rui, X. Wang, H. Ji, Catal. Today 258 (2015) 56–63.
[24] S.J. Park, I. Bae, I.-S. Nam, B.K. Cho, S.M. Jung, J.-H. Lee, Chem. Eng. J. 195 (2012) 392–402.
[25] X. Zou, Z. Rui, S. Song, H. Ji, J. Catal. 338 (2016) 192–201.
[26] Q. Fu, W.-X. Li, Y. Yao, H. Liu, H.-Y. Su, D. Ma, X.-K. Gu, L. Chen, Z. Wang, H. Zhang, Science 328 (2010) 1141–1144.
[27] M. Cargnello, J.D. Jaén, J.H. Garrido, K. Bakhmutsky, T. Montini, J.C. Gámez, R. Gorte, P. Fornasiero, Science 337 (2012) 713–717.
[28] R. Subbaraman, D. Tripkovic, K.-C. Chang, D. Strmcnik, A.P. Paulikas, P. Hirunsit, M. Chan, J. Greeley, V. Stamenkovic, N.M. Markovic, Nat. Mater. 11 (2012) 550–557.
[29] R. Subbaraman, D. Tripkovic, D. Strmcnik, K.-C. Chang, M. Uchimura, A.P. Paulikas, V. Stamenkovic, N.M. Markovic, Science 334 (2011) 1256–1260.
[30] G. Chen, Y. Zhao, G. Fu, P.N. Duchesne, L. Gu, Y. Zheng, X. Weng, M. Chen, P. Zhang, C.-W. Pao, J.-F. Lee, N. Zheng, Science 344 (2014) 495–499.
[31] Z. Rui, L. Chen, H. Chen, H. Ji, Ind. Eng. Chem. Res. 53 (2014) 15879–15888.
[32] A.P. Grosvenor, M.C. Biesinger, R.S.C. Smart, N.S. McIntyre, Surf. Sci. 600 (2006) 1771–1779.
[33] T.C. Deivaraj, W. Chen, J. Lee, J. Mater. Chem. 13 (2003) 2555–2560.
[34] L. Nie, A. Meng, J. Yu, M. Jaroniec, Sci. Rep. 3 (2013) 3215.
[35] X.D. Wang, H.B. Yu, D.Y. Hua, S.H. Zhou, J. Phys. Chem. C 117 (2013) 7294–7302.
[36] A.S. Ivanova, E.M. Slavinskaya, R.V. Gulyaev, V.I. Zaikovskii, O.A. Stonkus, I.G. Danilova, L.M. Plyasova, I.A. Polukhina, A.I. Boronin, Appl. Catal. B 97 (2010) 57–71.
[37] G. Busca, J. Lamotte, J.C. Lavalley, V. Lorenzelli, J. Am. Chem. Soc. 109 (1987) 5197–5202.
[38] J. Raskó, T. Kecskés, J. Kiss, J. Catal. 224 (2004) 261–268.
[39] R. Valentin, R. Horga, B. Bonelli, E. Garrone, F. Di Renzo, F. Quignard, Biomacromolecules 7 (2006) 877–882.
[40] G. Mekhemer, S. Halawy, M. Mohamed, M. Zaki, J. Phys. Chem. B 108 (2004) 13379–13386.